PERGAMON

International Journal of Solids and Structures 38 (2001) 6851–6867

INTERNATIONAL JOURNAL OF SOLIDS and STRUCTURES

www.elsevier.com/locate/ijsolstr

Genetic algorithm perspective to identify energy optimizing inclusions in an elastic plate

Shmuel Vigdergauz *

Research and Development Division, The Israel Electric Corporation Ltd., P.O. Box 10, Haifa 31000, Israel

Received 22 May 2000; in revised form 11 December 2000

Abstract

Analytical methods in optimization of elastic structures are often problematic due to the high order of the governing equations. It is therefore useful to try various numerical schemes in parallel to better understand the optimized object behavior. The paper describes the theoretical grounds and technical features that had to be introduced for effective implementation of a regular genetic algorithm (GA) to the shape optimization problems in planar elasticity. These features concern the fitness calculation and imposing specific geometric constraints as a way to drastically reduce the computational efforts. Finally we demonstrate a successful GA application for numerical shape optimization of a hole or rigid inclusion in a plate, arbitrarily loaded at infinity. Not only the known results have been reliably reproduced for the energy minimizing holes, but this approach has allowed us to extend the findings for the "worst" (energy maximizing) inclusions as well.

Keywords: Plane elasticity problem; Shape optimization; Effective energy; Kolosov–Muskhelishvili potentials; Extremal elastic structures; Equi-stress inclusions; Genetic algorithm

1. Introduction

Composites are becoming the material of choice in engineering today. Their greatest advantage is that they provide a designer with the ability of tailoring the effective material properties to a given external loading. This raises a number of recurring problems in elasticity, particularly the optimization of two-phase structures with respect to their energy stored at given average strains. The minimization of the strain energy leads to more rigid structures, with deflections and stresses considerably reduced.

The infinitely extended plane solid containing a single 1-connected inclusion is an often used scheme to model various problems of linear elasticity. This inclusion serves as an elementary discontinuity to disturb a homogeneous stress tensor $\sigma_0 = (\sigma^0_{xx}, \sigma^0_{yy}, \sigma^0_{xy})$ applied to the solid at infinity. Assuming additionally a

* Fax: +972-4-8649-770.
E-mail address: smuel@iec.co.il (S. Vigdergauz).

0020-7683/01/$ - see front matter
PII: S0020-7683(01)00017-8

perfect bonding along the phase interface, its shape remains the only factor controlling the stress distribution inside and around the inclusion. When the induced stress field provides the global energy minimum, the inclusion is referred to as energy minimizing or optimal for a taken loading. Concurrently, the opposite case of energy-maximizing inclusions is also of much interest, for together these extrema exactly bound the potential variety of the structures. Of special importance are the limiting structures when the inclusion has an infinite or zero rigidity.

Shape optimization is therefore a principal topic in structural design. For the 2D case, this problem was attacked mainly by analytical methods, such as the Kolosov–Muskhelishvily (KM) potentials (Muskhelishvili, 1975) combined with conformal mapping (see Vigdergauz, 1989; Haslinger and Dvořak, 1995, and references therein). In this way, an elliptic inclusion was shown to ensure the global energy minimum as defined by the known Gibiansky and Cherkaev (1986) analytical bounds. The ellipse orientation and eccentricity depend on the tensor σ_0, which should be sufficiently close to a hydrostatic loading (Vigdergauz, 1989, the exact formulation is given in Section 3). Additionally, such optimal inclusions exhibit an interesting local property of providing a uniform stress distribution along and inside the interface (the equi-stress boundaries, Vigdergauz, 1989). In the opposite case of dominating shear stresses, the situation is quite different. As it has been recently proved by Allaire and Aubry (1999) no non-degenerated inclusion shape can saturate the Gibiansky–Cherkaev bounds. However, a specific traction-free hole shape attaining a stationary energy value was semi-analytically found by Vigdergauz and Cherkaev (1986). Though distant from the global minimum, these sub-optimal shapes are important for understanding the optimization problem. Geometrically, they appeared to be very close to a rectangular with corners and slightly rounded sides, whose ratio depends on the far load. Moreover, the above-mention non-zero tangential stress has a constant absolute value almost everywhere on the contours except in the corners. When passing them the stress changes its sign discontinuously because of a discontinuous change of a tangent unit vector. This local property is referred to as *M*-(modular) equi-stressness (Vigdergauz and Cherkaev, 1986).

For further tackling the shape optimization problem, it seems reasonable to employ numerical methods in parallel.

Computationally, any optimization process involves two main ingredients: the solution of given boundary value problem (a direct problem) which has to be repeated many times, and a minimization scheme (an inverse or shape optimization problem). Here, the direct problem is governed by the high-order equations of elasticity, which must be handled numerically in a special way to provide a compromise between accuracy and efficiency.The associated inverse problem is known to be ill-posed, namely large changes of the contour can correspond to small changes in the stored energy. By this reason, traditional gradient-base optimization methods would require enormous calculations of the local stresses at each control point in contrast to the objective energy function easily evaluated by averaging the stress field. This discrepancy is especially pronounced for angular points that may drastically improve the performance of a candidate optimal shape as with the *M*-equi-stressness. Therefore, a more promising non-gradient alternative should be used when the search starts from different initial approximations, and proceeds according to some heuristic procedure.

In the attempt to overcome prohibitive numerical complexity of the problem at hand, we have applied here a genetic algorithm (GA) advanced by Goldberg (1989). The idea is simple: starting with a relatively small set of initial geometries, a number of structures that derive their properties from two of these individuals are generated. From this ''population'', the energetically ''most fit'' structures are chosen to replace their ''parents''. Repeating this process leads, as a rule, to extremal-energy structures.

GAs belong to the group of probabilistic searching methods that have a sufficient capability of locating the global optimum in the multidimensional searching space discarding all existing local optima. The robustness of the method, its ability to deal directly with optimization variables without any gradients and usage of an encoded binary representation of the modifiable variables are promising and advantageous.

GAs have been implemented to problems in many fields, but there have been only few successful applications to the full-scale theory of elasticity.

One of the difficulties here is that the evaluation of the energy by solving the direct problem is computer time consuming, especially when more accurate models are used. Our contribution to remedy the situation is two-fold. First, a new fast scheme of fitness evaluation is performed to improve the GA computational efficiency. This scheme may be easily incorporated in various numerical codes to solve other 2D elasticity problems as well. Second, we propose an effective self-adjusting encoding scheme to accomplish computational savings. Together with some other numerical tricks, this prevents us from calculating the energies of many thousands of non-competitive structures.

Further, due to its heuristic nature, one cannot apply the GA to the considered problem automatically. A reliable assessment of the numerical results may be only provided by comprehensive theoretical analysis in combination with the common sense considerations and even with the programming experience. With this in view, no wander that a high proportion of the paper is devoted to the required analytical preliminaries.

It should be noted however that no innovations are advanced in the genetic algorithm itself. The ordinary approach with integer genes and 1-point crossover turned out to be sufficient for our purposes. The real novelty is a fresh combination of the GA with comprehensive analytical study of the problem. By this reason, the paper is primarily intended to the elasticity rather than to the GA community.

In numerical experiments, our main attention has been paid to the case of pure shearing which plays significant role in the continual description of the mechanical properties of materials. In doing so, the GA appeared to be much more effective for holes and rigid inclusions than for elastic inhomogeneities. The closer the shear moduli of both materials are to each other, the less reliable the fitness computation.

The approach adopted here may serve as the first step in tuning the GA parameters and developing a numerical procedure that is appropriate for more general doubly periodic optimization problems. Such a procedure is currently under investigation.

The paper is organized as follows. In Section 2, we display some basic formulae in complex variable method of 2D elasticity. Section 3 states the optimization problem, while Section 4 describes the solution strategy based on the GA. In Section 5, we present not-too-standard encoding technique that automatically incorporate some geometrical constraint specifically pre-imposed on the moving interface to throw away most of the unpromising candidates. In Section 6, we discuss some computational issues related to the proposed scheme. The specific features of the optimization process are illustrated in Section 7 by a set of numerical examples. Comparison with results obtained by several different methods (when available) is also made to validate the method and demonstrate its performance. Finally, we make some concluding remarks in Section 8.

2. Governing equations of planar elasticity

Consider a thin infinite elastic plate containing a single non-identical inclusion with a closed boundary L. Locate a plate in the plane E of a complex variable $z = x + \mathrm{i}y$. The curve L divides the plane in two parts S_1 and S_2, $E = S_1 \cup S_2$, each occupied by its own linearly isotropic and homogeneous material with given bulk and shear moduli K_j, μ_j, $j = 1,2$.

Let the plate be remotely loaded by a uniform stress field σ_0 with the components $\sigma^0_{xx} = P_0$, $\sigma^0_{yy} = Q_0$ and $\sigma^0_{xy} = 0$ in the Cartesian coordinate system XOY. The stress state in E can be described using two pairs of KM potentials $\varphi_j(z)$, $\psi_j(z)$ (Muskhelishvili, 1975) which are complex-valued functions analytic respectively in the subdomains S_j, $j = 1,2$. These potentials are related to the stress tensor $\sigma = \{\sigma_{xx}, \sigma_{yy}, \sigma_{xy}\}$ and to the displacements $u_x(z) + \mathrm{i}u_y(z)$ at an arbitrary point in E by

$$\begin{aligned}
&\mathrm{Tr}\{\sigma(z)\} \equiv \sigma_{xx}(z) + \sigma_{yy}(z) = 4\mathrm{Re}\varphi_j'(z); \quad z \in S_j; \ \ j = 1,2\\
&\mathrm{Dev}\{\sigma(z)\} \equiv \sigma_{yy}(z) - \sigma_{xx}(z) = 2\mathrm{Re}\left[\bar{z}\varphi_j''(z) + \psi_j'(z)\right]\\
&\sigma_{xy}(z) = \mathrm{Im}\left[\bar{z}\varphi_j''(z) + \psi_j'(z)\right]
\end{aligned} \tag{2.1}$$

$$2\mu_j\big(u_x(z) + \mathrm{i}u_y(z)\big) = \lambda_j\varphi_j(z) - z\overline{\varphi_j'(z)} - \overline{\psi_j(z)}; \quad z \in S_j; \ \ j = 1,2 \tag{2.2}$$

Here $\lambda_j = 1 + 2\mu_j/K_j$, $j = 1,2$ is the Kolosov dimensionless constant (Muskhelishvili, 1975).

For further manipulations it is significant that the global part $\mathrm{Tr}\{\sigma(z)\}$ of the local stress tensor turns out to be independent of the second potential $\varphi_j(z)$ as seen from Eq. (2.1). Assuming perfect bonding at the matrix-inclusion interface, the potentials are linked to L through the continuity conditions (Muskhelishvili, 1975)

$$\varphi_1(t) + t\overline{\varphi_1'(t)} + \overline{\psi_1(t)} = \varphi_2(t) + t\overline{\varphi_2'(t)} + \overline{\psi_2(t)}; \quad t \in L \tag{2.3}$$

$$\mu_2\left(\lambda_1\varphi_1(t) - t\overline{\varphi_1'(t)} - \overline{\psi_1(t)}\right) = \mu_1\left(\lambda_2\varphi_2(t) - t\overline{\varphi_2'(t)} - \overline{\psi_2(t)}\right) \tag{2.4}$$

For definiteness, let the matrix related quantities be indexed with $j = 2$. Then the functions $\varphi_2(z)$, $\psi_2(z)$ satisfy the asymptotic requirements at infinity (Muskhelishvili, 1975)

$$\begin{aligned}
&\varphi_2(z) = B_2 z + \mathrm{O}\left(|z|^{-1}\right); \quad \psi_2(z) = \Gamma_2 z + \mathrm{O}\left(|z|^{-1}\right); \qquad |z| \to \infty\\
&4B_2 = P_0 + Q_0; \qquad 2\Gamma_2 = Q_0 - P_0
\end{aligned} \tag{2.5}$$

In parallel with (x,y) the polar coordinates (r,θ) will also be used, when needed. By the well-known (r,θ) to (x,y) transformation of the displacements and stresses (Muskhelishvili, 1975) we combine Eqs. (2.1), (2.2) and (2.5) to arrive at

$$\begin{aligned}
&\sigma_{rr}(z) = 2B_2 - \Gamma_2\cos 2\theta + \sigma_{rr}^-; \quad \sigma_{r\theta}(z) = \Gamma_2\sin 2\theta + \sigma_{r\theta}^-\\
&2\mu_2 u_r(z) = |z|[(\lambda_2 - 1)B_2 - \Gamma_2\cos 2\theta] + u_r^-; \quad 2\mu_2 u_\theta(z) = |z|\Gamma_2\sin 2\theta + u_\theta^-; \qquad |z| \to \infty
\end{aligned} \tag{2.6}$$

where the minus superscript denotes the items vanishing at infinity.

Identities (2.4)–(2.5) form the boundary value problem in the KM potentials $\varphi_j(z)$, $\psi_j(z)$, $j = 1,2$ which solves the medium stress state through Eqs. (2.1) and (2.2). Given far field Eq. (2.5), this problem is uniquely solvable for any fixed inclusion shape L (Muskhelishvili, 1975).

Of significant importance is also the attendant problem to find a *finite* perturbation ΔW of the *infinite* strain energy caused by the inclusion in the unbounded plate E. This quantity may be expressed (Muskhelishvili, 1975) as the limit of the convergent contour integral

$$2\Delta W = \int_0^{2\pi}\left[\sigma_{rr}u_r^- + \sigma_{r\theta}u_\theta^- - \sigma_{rr}^- u_r - \sigma_{r\theta}^- u_\theta\right]R\,\mathrm{d}\theta \tag{2.7}$$

taken over a circle with the radius R tending to infinity.

For further manipulation, we introduce the expansions (Muskhelishvili, 1975)

$$\varphi_1(z) = \sum_{k=0}^{\infty} a_k z^k; \quad \psi_1(z) = \sum_{k=0}^{\infty} b_k z^k; \qquad z \in S_1 + L \tag{2.8}$$

$$\varphi_2(z) = B_2 z + \Phi_2(z); \qquad \psi_2(z) = \Gamma_2 z + \Psi_2(z)$$
$$\Phi_2(z) = \sum_{k=1}^{\infty} a_{-k} z^{-k}; \quad \Psi_2(z) = \sum_{k=1}^{\infty} b_{-k} z^{-k}; \qquad z \in S_2 + L \tag{2.9}$$

that are valid for the KM potentials with the minimal smoothness requirements on the contour L. Note, that the constant terms with $k = 0$ are included in the expansions for φ_1, ψ_1. This choice is convenient but arbitrary because they correspond to the stress-free rigid body motion. The coefficients a_k and b_k, $k = 0, \pm 1, \pm 2, \ldots$, are given by the kth residues

$$a_k = \frac{1}{2\pi \mathrm{i}} \int_L \varphi_j(t) t^{-k-1} \, \mathrm{d}t; \quad b_k = \frac{1}{2\pi \mathrm{i}} \int_L \psi_j(t) t^{-k-1} \, \mathrm{d}t \qquad j = 1 \text{ for } k > 0; \quad j = 2 \text{ otherwise} \tag{2.10}$$

For convenient reference we display here the following identities (Muskhelishvili, 1977) that also hold for any closed curve L traversed in a counter-clockwise direction

$$\int_L t^n \mathrm{d}t = \begin{cases} 2\pi \mathrm{i}, & n = -1, \\ 0, & n = 0, 1 \pm 2, \pm 3, \ldots, \end{cases} \qquad \int_L \bar{t} \, \mathrm{d}t = 2\mathrm{i} c_1 \tag{2.11}$$

Here, c_1 stands for the inclusion area.

For dimensional reasons, the first coefficients a_{-1}, b_{-1} in Eq. (2.9) are proportional to c_1 (Muskhelishvili, 1977)

$$a_{-1} = \alpha_{-1} c_1; \qquad b_{-1} = \beta_{-1} c_1 \tag{2.12}$$

where the dimensionless quantities α_{-1}, β_{-1} depend on the interface shape and on the parameters involved

$$\alpha_{-1} = \alpha_{-1}(L, P_0, Q_0, K_1, \mu_1, K_2, \mu_2)$$
$$\beta_{-1} = \beta_{-1}(L, P_0, Q_0, K_1, \mu_1, K_2, \mu_2)$$

With Eqs. (2.6), (2.8) and (2.3), substituting Eqs. (2.8) and (2.9) into Eq. (2.7) yields after some algebra

$$\Delta W = 8\pi [2\Gamma_2 \alpha_{-1} + B_2 \beta_{-1}] \left(\frac{1}{K_2} + \frac{1}{\mu_2} \right) c_1 \tag{2.13}$$

At given phase moduli and load, the contour shape L remains the only factor controlling the stress distribution in the structure and hence its strain energy through α_{-1} and β_{-1}. Generally, these two unknowns are extracted as a by-product from the full-scale solution to the initial boundary problems (2.3) and (2.4) coupled with the asymptotics (2.5). In some instances, however, specific results may be reached by lesser efforts as shown in the next Section.

Remark. Relation (2.13) involves only the first terms of the expansion (2.9). It is not due to the single-inclusion approximation of the structure as might appear at first sight. A doubly periodic lattice of interacting inclusions yields the similar result (Vigdergauz, 1999) with the only difference that the powers of z are replaced by the Weierstrassian zeta-function and its derivatives to incorporate the translation properties of the KM potentials. The true reason is the averaging nature of the energy evaluation when the higher terms, though affecting α_{-1}, β_{-1} through the contact conditions (2.3) and (2.4) make no direct contribution in ΔW.

3. Problem formulation and analytical backgrounds

We are now in a position to address the optimization problem of finding the inclusion shape L that minimizes the energy perturbation

$$\Delta W \underset{\{L\}}{\rightarrow} \min \tag{3.1}$$

in relation to the parameters involved. For fixed far field σ_0, the minimum of ΔW obviously corresponds to a plate of maximum stiffness. Originally considered by Prager (1968), this problem was intensively studied for three last decades. To make the paper more self-contained, we summarize here some relevant known results together with new identities (3.15) and (3.16) especially derived for our purposes. Though lengthy, this Section provides a comprehensive theoretical basis required for reliable assessment of the numerical data obtained by the GA.

The problem is obviously hard to tackle by analytical methods. The main difficulty is that the sub-problems of finding the pairs $\varphi_1(z)$, $\psi_1(z)$ and $\varphi_2(z)$, $\psi_2(z)$ are closely intertwined by the contact conditions (2.3) and (2.4) and must, therefore, be treated simultaneously. However, on some interval of external loads an explicit solution may be found by application of the equi-stress concept (Vigdergauz, 1989), when the boundary sought L is so designed as to reduce the phase interaction to uniform normal stresses:

$$\sigma_{nn}^{(j)}(t) = \text{const.} = p_0; \quad \sigma_{n\tau}^{(j)}(t) = 0; \qquad j = 1,2; \;\; t \in L \tag{3.2}$$

where (n, τ) are the orthogonal curvilinear coordinates on L.

This makes it possible to decompose the initial problem of elasticity (2.3) and (2.4) into two less complicated sub-problems for each phase individually.

In doing so, we start with the prerequisite (3.2) and routinely develop the identities (2.1), (2.3) and (2.4) to arrive at (Vigdergauz, 1989)

$$2\varphi_1(z) \equiv p_0; \quad \psi_1(z) \equiv 0; \qquad z \in S_1 \tag{3.3}$$

$$\varphi_2(z) \equiv B_2 z; \quad z \in S_2 \tag{3.4}$$

and

$$\psi_2(t) = H_2 \bar{t}; \quad t \in L \tag{3.5}$$

where the real constants p_0, H_2 are defined by

$$p_0 = \frac{2\mu_1(\lambda_2+1)}{2\mu_1 + \mu_2(\lambda_1 - 1)} B_2; \qquad H_2 = p_0 - 2B_2 = 2\frac{\mu_1(\lambda_2 - 1) - \mu_2(\lambda_1 - 1)}{2\mu_1 + \mu_2(\lambda_1 - 1)} B_2 \tag{3.6}$$

With Eq. (2.1) it follows easily from Eq. (3.3) that the elastic field in the inclusion is homogeneous and pure spherical for *any* inclusion shape

$$\sigma_{xx}(z) = \sigma_{yy}(z) = p_0, \quad \sigma_{xy}(z) \equiv 0; \qquad z \in S_1$$

Next, substituting Eqs. (3.3) and (3.4) into expansions (2.8) and (2.9) yields

$$2a_1 = p_0; \quad a_k = 0; \;\; k \neq 1; \qquad b_k = 0; \quad k = 0, 1, 2, \ldots \tag{3.7}$$

The remaining identity (3.5) is then coupled with the second asymptotics (2.5) to pose the inverse boundary problem in finding a closed smooth curve on which the holomorphic function $\psi_2(z)$ takes the prescribed values.

This problem was shown solvable if and only if the parameters involved obey the inequality (Vigdergauz, 1989)

$$|\delta| \leqslant 1; \quad \delta = \frac{\Gamma_2}{H_2} \tag{3.8}$$

or, in equivalent terms

$$\left| \frac{\mathrm{Dev}\,\sigma_0}{\mathrm{Tr}\,\sigma_0} \right| = \left| \frac{P_0 - Q_0}{P_0 + Q_0} \right| \leqslant \left| \frac{\mu_2(\lambda_1 - 1) - \mu_1(\lambda_2 - 1)}{\mu_2(\lambda_1 - 1) + 2\mu_1} \right| \tag{3.9}$$

When this is the case, the contour sought is an ellipse of eccentricity δ aligned with the far field eigen-directions.

The inequality (3.9) implies that the deviatoric part Γ_2 of the remote field must be sufficiently small when compared to its spherical part B_2.

Now, the asymptotic coefficients α_{-1}, β_{-1} entering in Eq. (2.13) may be found explicitly to express the energy increment ΔW associated with equi-stress interfaces. With Eqs. (2.10) and (2.11) integration of Eq. (3.5) over L gives

$$\beta_{-1} = \pi^{-1} H_2 \tag{3.10}$$

while $\alpha_{-1} = 0$ in conformity with Eq. (3.7). Then recalling Eq. (3.6) we have

$$\Delta W = 8 B_2 H_2 \left(\frac{1}{K_2} + \frac{1}{\mu_2} \right) c_1 = \frac{\mu_1(\lambda_2 - 1) - \mu_2(\lambda_1 - 1)}{2\mu_1 + \mu_2(\lambda_1 - 1)} \mathrm{Tr}^2\,\sigma_0 \left(\frac{1}{K_2} + \frac{1}{\mu_2} \right) c_1 \tag{3.11}$$

When $\mu_2 \geqslant \mu_1$, this expression coincides with the global lower bound obtained by Gibiansky and Cherkaev (1986) thus proving the optimality of the equi-stress boundaries. In the opposite case of $\mu_2 \leqslant \mu_1$, the optimal problem formulation needs be changed so as that the remote strain tensor ε_0 is given instead of σ_0. Then, the equi-stress inclusions can be again proved optimal providing the largest possible compliance of the structure.

As a function of the elastic moduli, the allowed field anisotropy (3.9) ranges from all round compression ($P_0 = Q_0$) up to a uniaxial loading when only either of two principal stresses differs from zero:

$$0 \leqslant \left| \frac{\mathrm{Dev}\,\sigma_0}{\mathrm{Tr}\,\sigma_0} \right| \leqslant 1 \tag{3.12}$$

Here, the upper bound is reached in the limiting case of a hole ($\mu_1 = 0$) or rigid inclusion ($\mu_1 = \infty$). In such a situation, a rectilinear inhomogeneity oriented along the external loading really provides the optimal energy increment $\Delta W = 0$ because it brings no perturbation to the uniaxial external field.

Outside the range (3.9), the optimization problem (3.1) becomes much worse for the equi-stress principle is no longer applicable. As mentioned in Introduction, the only sub-optimal hole shape known thus far has a number of angular points. They permit the tangential stress $\sigma_{\theta\theta}$ to reverse its sign while remaining constant in magnitude (M-equi-stress contours, Vigdergauz and Cherkaev, 1986)

$$|\sigma_{\theta\theta}(t)| = \text{const.}; \quad t \in L \tag{3.13}$$

Unlike Eq. (3.2), the prerequisite Eq. (3.13) admits no analytical solution to the problem Eq. (3.1). By conformal mapping the numerical results were obtained by Vigdergauz and Cherkaev (1986) and more fully by Cherkaev et al. (1998). However, the energy increment ΔW turned out to be significantly higher than the global minimum

$$\Delta W = (Q_0 - P_0)^2 \left(\frac{1}{K_2} + \frac{1}{\mu_2} \right) c_1 \tag{3.14}$$

derived by Gibiansky and Cherkaev (1986) for a structure with one hyper-compliant phase ($\mu_1 = 0$). Recently it has been proved by Allaire and Aubry (1999) that no simple-connected hole may saturate the

bound (3.14). But here the question arises of whether the M-equi-stress hole shape parallels (3.14) more closely than any other non-degenerated curve does. Using the GA numerical procedure we answer affirmative (Section 7).

Surprisingly, the key relation (3.5) admits a closed-form solution for the stresses induced by an elliptic inclusion in any remote field $Q, P = qQ, -\infty \leqslant q \leqslant \infty$ (Vigdergauz, 1989). In order to save room, we display here only the resultant expression for the energy increment when $\mu_1 = 0$

$$\Delta W = \frac{2(\delta B - \Gamma) + [(1+\delta)B + \Gamma](1-\delta)B}{4(\delta^2 - 1)} \left(\frac{1}{K_2} + \frac{1}{\mu_2}\right) c_1 \quad B = P + Q; \;\; \Gamma = Q - P$$

Again, δ denotes the ellipse eccentricity.

Negative values of the parameter q correspond to the shear-type remote loading when the principal stresses P, Q have the opposite signs. To be more specific we put $-1 \leqslant q \leqslant 0$ and hence $|P| \leqslant |Q|$ or equivalently $|B| \leqslant |\Gamma|$. Then, as a function of δ, the energy takes the minimum value

$$\min_{0 \leqslant \delta \leqslant 1} \Delta W = \Delta W = \frac{2\Gamma^2 - B^2}{4} c_1 \left(\frac{1}{K_2} + \frac{1}{\mu_2}\right) \tag{3.15}$$

at the point

$$\delta = |B/\Gamma| \leqslant 1 \tag{3.16}$$

Remark. When compared to (3.8) the last relation implies that the elliptic inclusion which provides the optimum (3.11) for the bulk-type remote loading P_0, Q_0, $P_0 Q_0 \geqslant 0$ is likewise optimal for its anisotropic complement P_0, $-Q_0$, $P_0 Q_0 \leqslant 0$. Of course, the geometrically independent and thus global estimate (3.11) is distinguished from the minimum (3.15) locally taken over all possible ellipses.

Relations (3.14) and (3.15) form a two-sided bound on the energy minimum over all non-degenerated holes. They merge in the above-mentioned limiting case of the uniaxial loading ($q = 0$). As is shown numerically in Section 7, the smallest possible values of ΔW fall rather closely to the upper bound (3.15).

To gain a better understanding of the phase interplay in the optimization process, it is also desirable to identify the "worst" inclusion shapes that provide a maximum value of ΔW. Not considered before they may be found by the GA with equal ease. In doing so non-concave curves alone are studied to weed out star-shaped inclusions with many needles that store an arbitrary large energy.

4. The genetic algorithm outline

GAs are adaptive search strategies inspired by Darwin's theory of evolution. They mimic the mechanism of natural evolution, hereditary and survival of the fittest. Each potential solution is discretely encoded in a data string. A population of such individuals is initially created at random. Then pairs of individuals cross over at a random point of the string to produce a descendant for the next generation. A mutation process is also used to randomly modify the genetic structure of some members of each new generation. The probability of an individual reproducing is proportional to the fitness of solution it presents. Consequently, the quality of the solutions in successive generations improves "automatically" keeping only the fittest individuals from the past generation in subsequent populations.

The process is terminated when an acceptable or optimum solution is found, or after some fixed computing time limit. This iterative scheme is appropriate for problems that require optimization with respect to some computable criterion. Mathematically, GAs are not always well based, but this heuristic technique

has shown its efficiency in a number of fields including elasticity (see, for instance Schoenauer et al., 1997 and references therein).

5. Design variables and boundary representation

In conformity with Eqs. (2.12) and (2.13) the normalized fitness of individuals assumes the form

$$F=\frac{2(1-q)(\lambda_2-1)a_{-1}+(1+q)b_{-1}}{c_1};\quad q=\frac{P_0}{Q_0};\ \ Q_0\neq 0 \tag{5.1}$$

Numerically, the optimal inclusion shape depends on the discrete boundary representation of an admissible interface through a finite number of the design variables. Due to the adopted symmetry, they are taken only in the first quadrant $0\leqslant\theta\leqslant\pi/2$ of the plane. Further, the problem is scale-independent so we may fixed the contour at the point $z_0=1$ to prevent shrinkage. The remaining design variables are radial coordinates of M control points $z_m=r_m\exp(\mathrm{i}\pi m/2M)$, $m=1,2,3,\ldots,M$, equally spaced on the irreducible portion of L. Their proper representation in the search space is greatly important for the GA to be successfully employed in the structural optimization.

Here, the variables are encoded using a discrete n-bits procedure as exemplified in Fig. 1 for $n=8$. Namely, the radius r_m is approximated only by 2^n values in the continuous search space $\left[r_m^{(\min)};r_m^{(\max)}\right]$. For example, the binary string 10010011 (Fig. 1) returns the mth control point to the decimal position $D_m=1*2^7+0*2^6+0*2^5+1*2^4+0*2^3+0*2^2+1*2^1+1*2^0=147\in[0;2^n-1]$ so that

$$r_m=r_m^{(\min)}+\frac{D_m}{2^n-1}\left(r_m^{(\max)}-r_m^{(\min)}\right)=r_m^{(\min)}+\frac{147}{255}\left(r_m^{(\max)}-r_m^{(\min)}\right) \tag{5.2}$$

The candidate representation consists in concatenating all M variables to form one long string or chromosome. The inverse decoding process returns decimal values of the radii that are necessary to calculate the fitness F.

Early in the process, the GA searches for the optimum in an undirected way and thus spends too much time to estimate obviously unpromising candidates. To keep the GA from generating such chromosomes we use the intuitive consideration by which the optimal contour may not be concave. This assumption, while not proved mathematically, is justified for all solutions known so far. Another reasoning suggests that the larger of two stresses P_0, Q_0 should elongate the contour in its own direction. For definiteness, let this be the y-axis and thereby $|P|<|Q|$ or, equivalently, $|q|<1$. With the fixed point $z_0=1$, the contour then contains a unit rhombus $(1,\mathrm{i},-1,-\mathrm{i})$ at least. Both constraints are incorporated into the encoding procedure by specially defining the intervals $\left[r_m^{(\min)};r_m^{(\max)}\right]$ in the following way. As is shown in Fig. 2, the first design parameter r_1 varies between the radial coordinates of two points at which the current ray meets the side AB of the rhombus and the perpendicular AC to the x-axis. Each successive control variable r_m, $m=2,3,\ldots,M$

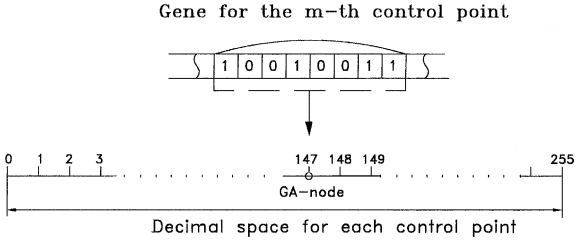

Fig. 1. Shape encoding procedure.

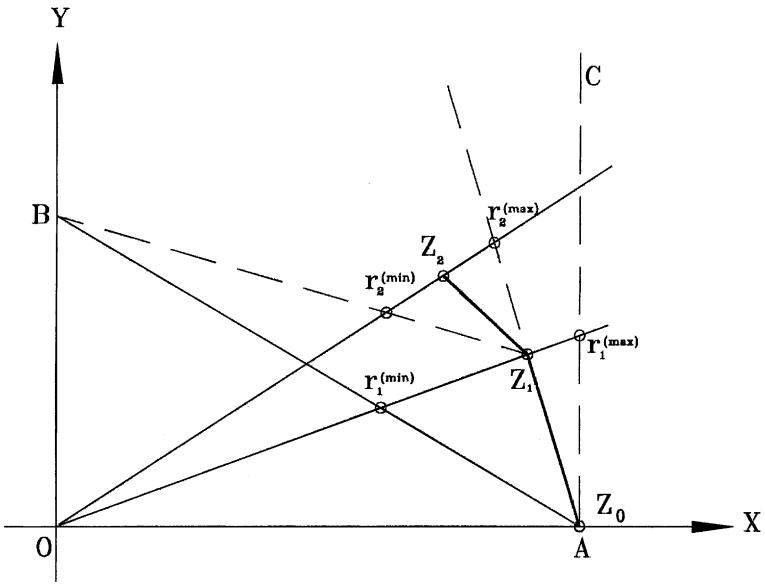

Fig. 2. Step-by-step scheme of self-adjusting convexity.

is bounded on the corresponding ray by intersections with two specific lines. The first line DB (see Fig. 2) goes through the preceding control point z_{m-1} and the corner B to keep the contour from meeting with the rhombus. Extending the previous segment z_{m-1}, z_{m-2} we draw the second constraint line DE that provides non-concavity of the contour at the current point z_m. Each interval $\left[r_m^{(\min)}; r_m^{(\max)}\right]$, $m = 2, 3, \ldots, M$ thus depends on randomization of all the preceding points. Though not quite straightforward, this chain scheme effectively restricts the analysis to a much smaller set of opportunities.

6. Computational preliminaries

As already noted, only the first terms a_{-1}, b_{-1} of the expansions (2.9) appear in the energy criterion (2.13). However, they may not be found independently of the other coefficients a_k, b_k, $k = 0, 1, \pm 2, \ldots$ which are intertwined by the contact conditions on L. Therefore, the fitness evaluation of each member in the genetic population must be performed by solving the full-scale boundary value problem (2.3) and (2.4). With Eq. (2.5), these relations may be rearranged for later use as

$$\varphi_1(t) + t\overline{\varphi_1'(t)} + \overline{\psi_1(t)} - \Phi_2(t) - t\overline{\Phi_2'(t)} - \overline{\Psi_2(t)} = 2B_2 t + \Gamma_2 \bar{t}; \quad t \in L \tag{6.1}$$

$$\mu_2\left(\lambda_1\varphi_1(t) - t\overline{\varphi_1'(t)} - \overline{\psi_1(t)}\right) - \mu_1\left(\lambda_2\Phi_2(t) - t\overline{\Phi_2'(t)} - \overline{\Psi_2(t)}\right) = \mu_1 B_2(\lambda_2 - 1)t - \mu_1\Gamma_2\bar{t} \tag{6.2}$$

Substituting the expansion (2.8), (2.9) into Eqs. (6.1) and (6.2) leads, in one way or another, to an infinite system of linear algebraic equations for the unknowns a_k, b_k, $k = 0, \pm 1, \pm 2, \ldots$. Of course, in practice this infinite system is truncated and replaced by a finite linear system which includes only the first N unknowns, for a certain finite N. One of the difficulties in solving the direct elasticity problem (6.1) and (6.2) is that the truncated system may be ill-conditioned. In this case GAs become poorly unstable and the searching trajectory starts to move away from a feasible optimum.

The geometrical limitations outlined in the previous section serve not only to save computational efforts but also to exclude the "stubborn" structures whose quantitative assessment is problematic by the above reason.

The situation can be further improved by properly manipulating the problem equations, because, at a given contour L, computational properties of the system partially depend on how it has been analytically derived from Eqs. (6.1) and (6.2). Despite a variety of numerical schemes, it is not easy to find an accurate method yet matching the stringent GA requirements on the memory, speed and computational stability. Therefore, our main concern is to simplify the system structure as much as possible. This may be achieved through the same identities (6.1) and (6.2) which give no way of separating the coefficients sought a_{-1}, b_{-1}. When properly used, they admit of solving the pairs of the KM potentials $\varphi_2(z)$, $\varphi_1(z)$ and $\psi_2(z)$, $\psi_1(z)$ individually, with the latter obtained by straightforward integration. The idea goes back to Sherman (see Muskhelishvili, 1975) who derived a regular integral equation in only one complex-valued function $\varphi_2(t)$ on L. After solving the equation, the second potential $\psi_2(z)$ is given by the Cauchy integral of the expression $\overline{\varphi_2(t)} - \bar{t}\varphi_2'(t)$ over L especially tailored to satisfy traction-free boundary conditions. Therefore, the Sherman equation is applicable only for a plate with holes. When elastic inclusions are taken instead, its counterpart, though singular, has recently been obtained by Greengard and Helsing (1998). Interestingly the singular term vanishes when both phases have the same bulk modulus. Both equations were used in practice to solve the direct problem of elasticity (Vigdergauz, 1974; Greengard and Helsing, 1998). Here this approach is modifies in the following way.

First, let us rearrange the Eqs. (6.1) and (6.2) separating out the functions $\psi_1(t), \Psi_2(t)$

$$(\mu_1 - \mu_2)\psi_1(t) = \mu_1(\lambda_2 + 1)\overline{\Phi_2(t)} - (\mu_1 + \mu_2\lambda_2)\overline{\varphi_1(t)} + (\mu_2 - \mu_1)\bar{t}\varphi_1'(t) + \mu_1(\lambda_2 + 1)B_2\bar{t}; \quad t \in L \tag{6.3}$$

$$\begin{aligned}(\mu_1 - \mu_2)\Psi_2(t) = {} & (\mu_2 + \mu_1\lambda_2)\overline{\Phi_2(t)} + (\mu_2 - \mu_1)\bar{t}\Phi_2'(t) - \mu_2(\lambda_1 + 1)\overline{\varphi_1(t)} + [\mu_1(\lambda_2 - 1) + 2\mu_2]B_2\bar{t} \\ & + (\mu_2 - \mu_1)\Gamma_2 t; \quad \mu_1 \neq \mu_2\end{aligned} \tag{6.4}$$

Next, we consider the following Cauchy integral

$$\int_L \frac{\omega_1(t)}{t - z}\mathrm{d}t \equiv 0; \quad z \in S_2 \tag{6.5}$$

that holds for any function $\omega_1(z)$ holomorphic in S_2.

Expanding the Cauchy kernel into a convergent power series in t

$$\frac{1}{t - z} = -\frac{1}{z\left(1 - \frac{t}{z}\right)} = \frac{1}{z}\sum_{j=0}^{\infty}\left(\frac{t}{z}\right)^j; \quad \left|\frac{t}{z}\right| < 1; \ z \in S_2 \tag{6.6}$$

we substitute Eq. (6.6) in Eq. (6.5) to obtain

$$\int_L \omega_1(t)t^j\mathrm{d}t = 0; \quad j = 0, 1, \ldots \tag{6.7}$$

In a like manner, the following identities may be derived for an arbitrary function $\omega_2(z)$ holomorphic in S_2 and vanishing at infinity

$$\int_L \omega_2(t)t^{-j-1}\mathrm{d}t = 0; \quad j = 0, 1, \ldots \tag{6.8}$$

Finally, we multiply both sides of Eqs. (6.3) and (6.4) by t^n, $n = 0, 1, 2, \ldots$, and $n = -1, -2, \ldots$, respectively. Using the expansions (2.9) we write the integrals (6.7) and (6.8) term by term to obtain the system of a halved size involving only the coefficients a_k, $k = 0, \pm 1, \pm \ldots$.

$$\sum_{k=0}^{\infty} C_{k,j}^{1,-1} a_{-k} + \sum_{k=0}^{\infty} C_{k,j}^{1,1} a_k = D_j^{(1)}; \quad j = 0, 1, 2, \ldots$$
$$\sum_{k=0}^{\infty} C_{k,j}^{2,-1} a_{-k} + \sum_{k=0}^{\infty} C_{k,j}^{2,1} a_k = D_j^{(2)} \tag{6.9}$$

where the matrix entries and the right-hand side take the unified form

$$C_{0,j}^{1,-1} = 0; \qquad C_{k,j}^{1,-1} = \mu_1(\lambda_2 + 1) J_{-k,j}; \quad k \geqslant 1$$
$$C_{k,j}^{1,1} = (\mu_1 + \mu_2\lambda_2) J_{k,j} + (\mu_2 - \mu_1) k J_{1,k+j}$$
$$C_{k,j}^{2,-1} = (\mu_2 + \mu_1\lambda_2) J_{-k,-j} + (\mu_2 - \mu_1) k J_{1,-k-j} \tag{6.10}$$
$$C_{k,j}^{2,1} = -\mu_2(\lambda_1 + 1) J_{k,-j}$$
$$D_j^{(1)} = -\mu_1(\lambda_2 + 1) B_2 J_{1,j}; \qquad D_j^{(2)} = -(\mu_1(\lambda_2 - 1) + 2\mu_2) B_2 J_{1,-j-1} + (\mu_2 - \mu_1) \Gamma_2 J_{0,-j-1}$$

Here $J_{k,l}$ stands for the regular integral over L

$$J_{k,j} = \int_L \overline{t}^k t^j \mathrm{d}t; \quad k, j = 0, \pm 1, \pm 2, \ldots; \ k \neq j \tag{6.11}$$

These integrals are evaluated numerically, except in a few special cases

$$J_{0,-1} = 2\pi\mathrm{i}; \quad J_{0,j} = 0; \quad j \neq -1; \quad J_{1,0} = 2\mathrm{i}c_1$$

as given by Eq. (2.11).

Once a_k, $k = 0, \pm 1, \pm \ldots$ are found, we substitute them back to Eq. (6.4) and integrate over L to obtain the coefficient b_{-1} also involved in the criterion (2.13) for $B_2 \neq 0$

$$(\mu_1 - \mu_2) \int_L \Psi_2(t)\, \mathrm{d}t = 2\pi\mathrm{i} b_{-1}$$
$$= (\mu_2 + \mu_1\lambda_2) \sum_{k=1}^{\infty} a_{-k} \int_L \overline{t^{-k}} \mathrm{d}t + (\mu_1 - \mu_2) \sum_{k=1}^{\infty} k a_{-k} \int_L \overline{t} t^{-k-1} \mathrm{d}t - 2\mathrm{i}\mu_2(\lambda_1 + 1) c_1$$
$$- \mu_2(\lambda_1 + 1) \sum_{k=2}^{\infty} a_k \int_L \overline{t}^k \mathrm{d}t + 2\mathrm{i}[\mu_1(\lambda_2 - 1) + 2\mu_2] B_2 c_1; \quad \mu_1 \neq \mu_2 \tag{6.12}$$

This completes the solution of the direct problems (6.1), (6.2).

Further computational savings may be achieved by letting the contour L be symmetric about the x- and y-axes of the coordinate system and centered at its origin. Then, due to the rotational properties of the KM potentials (Muskhelishvili, 1975), the coefficients (2.10) having odd indices are real while the rest vanish. The system (6.9) is likewise real with the integrals (6.11) taken only along the one fourth of the contour.

Clearly the KM potentials $\varphi_1(z)$, $\psi_1(z)$ vanish identically in S_1 for holes or rigid inclusions. Hence the relations (6.1) and (6.2) reduced to the form

$$\psi_2(z) = \lambda_2 \overline{\varphi_2(z)} - \overline{t} \varphi_2'(z)$$

where we should formally put $\lambda_2 = -1$ for holes (the Dundurs correspondence, Jasiuk, 1995). The resultant algebraic system of linear equations in a_k, $k = -1, -2, \ldots$ is not written here to save room.

7. Numeric results

It is commonly known that good use of GA can be made only with the proper choice of heuristic parameters involved such as the population size, mutation rate and some others. Literature reports various and discrepant data. Because of this, we first calibrate the approach by numerically reproducing the optimality relation (3.10) of the equi-stressness for ellipses. On putting $\sigma_{yy}^{\infty}=1$ in Eqs. (2.5) and (3.6), this identity becomes especially simple when $\mu_1=0$ (elliptical holes)

$$\alpha_{-1}^{(\mathrm{hole})}=0;\quad 2\pi\beta_{-1}^{(\mathrm{hole})}=1+q;\qquad \sigma_{\theta\theta}^{(\mathrm{hole})}(t)=1+q;\quad \sigma_{rr}^{(\mathrm{hole})}(t)=0;\ \ t\in L \tag{7.1}$$

or $\mu_1=:$ (elliptical rigid inclusions)

$$\begin{aligned}&\alpha_{-1}^{(\mathrm{rigid})}=0;\quad 4\pi\beta_{-1}^{(\mathrm{rigid})}=-(\lambda_2-1)(1+q);\\&4\sigma_{\theta\theta}^{(\mathrm{rigid})}(t)=(3-\lambda_2)(1+q);\quad 4\sigma_{rr}^{(\mathrm{rigid})}(t)=(1+\lambda_2)(1+q);\qquad t\in L\end{aligned} \tag{7.2}$$

In accordance with (3.12) the above relations are valid in the interval $0\leqslant q\leqslant 1$. To make the results more observable we display only the average stress $\langle\sigma_{\theta\theta}\rangle$ taken over the nodes along the equi-stress boundary. For a circle ($q=0$) the mean value $\langle r\rangle$ of all r_m, $m=1,2,3,\ldots,M$ is also computed to evaluate the out-of-roundness. Since $r_0=1$ the exact value of $\langle r\rangle$ is unity too.

Table 1 shows the stable values of the above parameters obtained by averaging over 10 independent optimizations, each including up to 300 iterations. Due to the problem rotational symmetry, the control points are located only in the portion of the curve L bounded by the angle $0\leqslant\theta\leqslant\pi/4$. Apart from the coefficient $\alpha_{-1}^{(\mathrm{hole})}$, all the parameters are normalized by their exact non-zero values though we use the same notations for convenience. Table 2 lists their standard deviations computed at $M=30$ and $N=14$. A typical convergence characteristic for the GA scheme is shown in Fig. 3. Considering the complexity of the problem, convergence was obtained in remarkably small number of iterations.

Table 3 presents the set of numerical data, which simulates the identities (7.2) for a rigid ellipse of eccentricity $\delta_{\mathrm{e}}=q$ over the interval of loads $0\geqslant q\geqslant 0.4$. As against the previous case, the number M of the control points is doubled here to space them in the angle $0\leqslant\theta\leqslant\pi/2$ with the same step. It is worth noting that the energy-related parameters are approximated substantially better than the stresses and contour geometry. Our experience suggests that a higher accuracy is arrived at by refining the contour

Table 1
Normalized constants $\alpha_{-1}^{(\mathrm{hole})}$, $\pi\beta_{-1}^{(\mathrm{hole})}$, $\langle\sigma_{\theta\theta}\rangle$ and $\langle r\rangle$ versus the number M of control variables and the system size N

Parameter	$M=15$	$M=30$	$M=45$	
ΔW	1.0000777	1.0000430	1.0000956	$N=7$
$\alpha_{-1}^{(\mathrm{hole})}\times 10^4$	3.0566734	2.9844509	2.6604456	
$\beta_{-1}^{(\mathrm{hole})}$	0.9989623	0.9986322	0.9985533	
$\langle\sigma_{\theta\theta}\rangle$	1.0034427	1.0027765	1.0035898	
$\langle r\rangle$	0.9989700	0.9986073	0.9985399	
ΔW	1.000006	1.0000000	1.0000011	$N=14$
$\alpha_{-1}^{(\mathrm{hole})}\times 10^5$	4.0677631	3.7719578	3.6323497	
$\beta_{-1}^{(\mathrm{hole})}$	0.9999800	0.9999755	0.9999664	
$\langle\sigma_{\theta\theta}\rangle$	1.0009566	1.0000767	1.0000944	
$\langle r\rangle$	0.9999950	0.9999761	0.9999824	
ΔW	1.0000000	1.0000000	1.0000000	$N=21$
$\alpha_{-1}^{(\mathrm{hole})}\times 10^6$	4.5460993	4.4872343	4.2672398	
$\beta_{-1}^{(\mathrm{hole})}$	1.0000010	1.0000009	1.0000000	
$\langle\sigma_{\theta\theta}\rangle$	0.9998566	1.0000569	1.0000867	
$\langle r\rangle$	1.0000007	1.0000011	1.0000006	

Table 2
Standard deviations of the optimum-related parameters taken for $M = 30$ and $N = 14$ over 10 optimizations

Parameter	Standard deviation
ΔW	2.1320×10^{-6}
$\alpha_{-1}^{(\text{hole})}$	4.8446×10^{-5}
$\beta_{-1}^{(\text{hole})}$	6.4959×10^{-5}
$\langle \sigma_{\theta\theta} \rangle$	5.3330×10^{-3}
$\langle r \rangle$	1.5569×10^{-3}

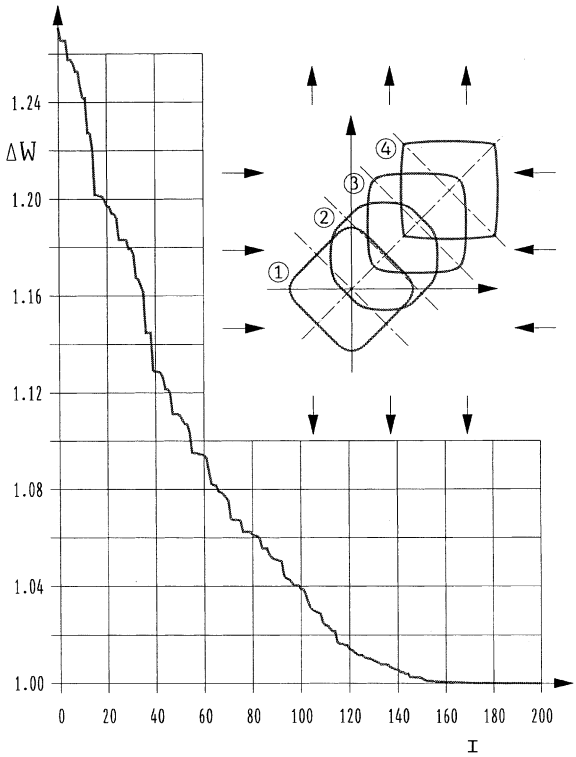

Fig. 3. The optimization history of the normalized energy F from Eq. (5.1) and the hole shape evolution for pure shear loading against the number of iterations: $I = 10$ (a), 50(b), 100(c), 150(d).

Table 3
Normalized constants ΔW, $\alpha_{-1}^{(\text{rigid})}$, $\pi\beta_{-1}^{(\text{rigid})}$ and the ellipse axes ratio R_e versus the loading parameter q. The number of control points M and the system size N are taken as 60 and 14 correspondingly[a]

Constant	$q = 1.0$	$q = 0.8$	$q = 0.6$	$q = 0.4$
ΔW	1.00000	1.00000	1.00000	1.00006
$\alpha_{-1}^{(\text{hole})} \times 10^{-4}$	4.03298	4.78450	5.73987	7.90563
$\beta_{-1}^{(\text{hole})}$	1.00000	1.00004	1.00010	1.00048
$\langle \sigma_{\theta\theta} \rangle$	1.00407	1.00662	1.02080	1.04043
R_e	1.00282	1.00907	1.01210	1.02065

[a] Theoretically, $R = (1 - \delta)/(1 + \delta) = q$ as dictated by Eq. (3.8).

Table 4
The GA parameter values used in further optimizations

GA parameter	Parameter value(s)
Gene	Integer number [0; 255]
Individual	Interface shape
Population size	1000
Number of genes	91
Initial population	1000 arbitrarily generated individuals
Selection	Ranking
Elitism	Four best individuals
Crossover	1-point
Crossover rate	0.90
Creep mutation	By randomly changing a bit
Creep mutation rate	0.35
Jump mutation	By adding a random integer value typically [−4; 4]
Jump mutation rate	0.35

discretization. In addition, increasing the computational size of the direct problem may also improve the stress values once the optimal shape is identified.

In our opinion, these results are an important test of the optimization technique: they reliably reproduce all of the known low-energy structures. They are used as a benchmark to choose the GA parameter values summarized in Table 4. Here and henceforth, the stopping criterion for all set of runs was fixed at 400 iterations.

We next identify the high-energy structures for $q = 1$ (hydrostatic loading) and for $q = -1$ (pure shear). Both contours were found to be a true square (at $q = -1$ rotated through 90°) which is not displayed here to save room. A number of the related data are collected in Table 5. It should be noted that the energy increment values F defined by Eq. (5.1) are obtained by Jasiuk (1995) in all cases by solving the *direct* rather than the *optimal* elasticity problem. The computed minimum of F at $q = -1$ and its counterpart from Vigdergauz and Cherkaev (1986) and from Cherkaev et al. (1998) are also added for reference.

All these pairs of extrema are rather close to each other. This is because only convex curves with four-fold rotational symmetry were taken to compute the maximum values. In response, the GA arrives at straight-line segments that close the admissible contour set. As mentioned in the end of Section 3, strictly concave contours may store an arbitrarily large strain energy in re-entrant corners.

Finally, the optimal hole shapes have been identified for asymmetric shear loading when $0 \geqslant q \geqslant -1$. As expected, they look like rectangles with the slightly rounded sides whose ratio specifically depends on q. Fig. 4 exhibits the associated energy increment F versus the parameter q. The bounds (3.14) and (3.15) are also given for comparison.

8. Closure and future applications

When applied to the full-scale shape optimization problems in elasticity the GA exhibits the low computational efficiency due to the high-order governing equations. The main goal of this work was to try a solution strategy consisting of a new effective numerical code of fitness computation and simple modifications in the encoding procedure freshly combined with the basic structure of the GA. This approach was used to effectively solve the 2D optimization problem for elastic plates with a dilute concentration of holes or rigid inclusions.

In order to make the GAs more competitive with traditional optimization tools, further research must be conducted to check their efficiency. In doing so, it is important to precede the GA computations by a

Table 5
The computed extrema of the energy increment ΔW in comparison with the literature values[a]

	Hydrostatic loading ($q = 1$)				Pure shear ($q = -1$)			
	Hole		Rigid inclusion		Hole		Rigid inclusion	
	Min	Max	Min	Max	Min	Max	Min	Max
	1.0000	1.1935	−2.0000	−2.2693	1.8541	2.6597	−1.1041	−0.9455
Cherkaev et al. (1998)	1.0000		−2.0000		1.8573			
Jasiuk (1995)	1.0000	1.1818	−2.0000	−2.2554	1.8702	2.6182	−1.1422	−0.9725

[a] For rigid inclusions ($\mu_1 = \infty$) we put the Poisson ratio of the plate $\nu_2 = 0.3$.

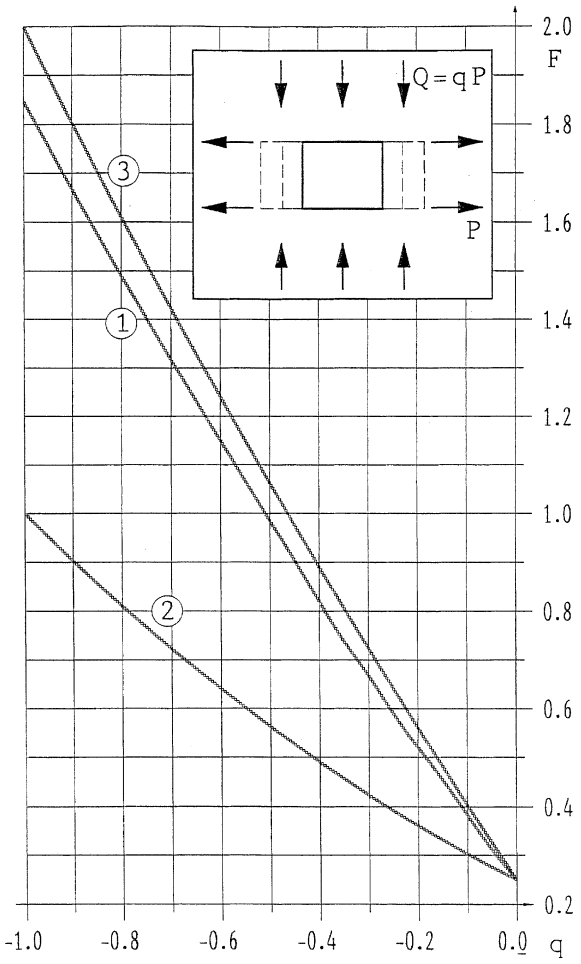

Fig. 4. The energy increment for the optimal hole under shear-type loading (1) bounded by the estimates (3.14) and (3.15) (the curves 2 and 3, correspondingly).

comprehensive theoretical analysis. The conducted study demonstrates that a combination of analytical and numerical methods of investigating optimization problems allows for the effective use of the best features of both approaches. It would be thus interesting to apply this dual approach to study regular

composites with non-generated foreign inclusions that exhibit optimal response on the shear loading. Theoretically, the situation here is the same as in the case of one inclusion approximation: equi-stress interfaces were identified analytically as a global minimum if the average field is rather isotropic (see Vigdergauz, 1999 and references therein), otherwise no results are obtained so far. We currently adapt the genetic algorithm to tackle this doubly periodic problem.

References

Allaire, G., Aubry, S., 1999. On optimal microstructures for a plane shape optimization problem. J. Struct. Optimiz. 17, 86–94.

Cherkaev, A.V., Grabovsky, Y., Movchan, A.V., Serkov, S.K., 1998. The cavity of optimal shape under shear stresses. Int. J. Solids Struct. 35, 4391–4410.

Gibiansky, L.V., Cherkaev, A.V., 1986. Design of composite plates of extremal rigidity. Report 914, A.F. Ioffe. Phys. Tech. Inst., Acad. of Sci., Leningrad, USSR (English Transl.: Cherkaev, A.V., Kohn, R.V. (Eds.), 1997. Topics in the Mathematical Modelling of Composite Materials. Birkhauser, Boston).

Goldberg, D.E., 1989. Genetic Algorithms in Search, Optimization and Machine Learning. Addison-Wesley, Reading, MA.

Greengard, L., Helsing, J., 1998. On the numerical evaluation of elastostatic fields in locally isotropic two-dimensional composites. Int. J. Mech. Phys. Solids. 46, 1441–1462.

Haslinger, J., Dvořak, J., 1995. Optimum composite material design. Math. Mod. Num. Anal. 29, 657–686.

Jasiuk, I., 1995. Cavities vis-a-vis rigid inclusions: elastic moduli of materials with polygonal inclusions. Int. J. Solids Struct. 32, 407–422.

Muskhelishvili, N.I., 1975. Some Basic Problems of the Mathematical Theory of Elasticity. Noordhoff, Leiden, The Netherlands.

Muskhelishvili, N,I., 1977. Singular Integral Equations. Noordhoff International, Leiden.

Prager, W., 1968. Optimality criteria in structural design. Proc. Nat. Acad. Sci. USA. 61, 794–796.

Schoenauer, M., François, J., Kallel, L., 1997. Identification of mechanical inclusions. In: Dasgupta, D., Michalewicz, Z. (Eds.), Evolutionary Algorithms in Engineering Applications, Springer, Heidelberg.

Vigdergauz, S.B., 1974. The problem of elasticity for multiconnected regions with cyclic symmetry. J. Appl. Math. Mech. 38, 522–525.

Vigdergauz, S.B., Cherkaev, A.V., 1986. A hole in a plate optimal for its biaxial extension-compression. J. Appl. Math. Mech. 50, 401–404.

Vigdergauz, S.B., 1989. Piecewise-homogeneous plates of extremal stiffness. J. Appl. Math. Mech. 53, 76–80.

Vigdergauz, S.B., 1999. Complete elasticity solution to the stress problem in a planar grained structure. Math. Mech. Solids 4, 407–441.